IVYSPRING INTERNATIONAL PUBLISHER

Theranostics

2017; 7(2): 357 -376. doi: 10.7150/thno.16855

Research Paper

Systemic siRNA Delivery with a Dual pH-Responsive and Tumor-targeted Nanovector for Inhibiting Tumor Growth and Spontaneous Metastasis in Orthotopic Murine Model of Breast Carcinoma

Bo Fan[1,3], Lin Kang[1], Liqing Chen[1], Ping Sun[1], Mingji Jin[1], Qiming Wang[1], You Han Bae[2], Wei Huang[1]✉, Zhonggao Gao[1]✉

1. State Key Laboratory of Bioactive Substance and Function of Natural Medicines, Department of Pharmaceutics, Institute of Materia Medica, Chinese Academy of Medical Sciences and Peking Union Medical College, Beijing 100050, PR China.
2. Department of Pharmaceutics and Pharmaceutical Chemistry, College of Pharmacy, University of Utah, Rm 2972, Skaggs Pharmacy Institute, 30S 2000E, Salt Lake City, Utah 84112, USA.
3. School of Pharmaceutical Science, Shanxi Medical University, No. 56, Xinjian Nan Road, Taiyuan 030001, Shanxi, People's Republic of China.

✉ Corresponding authors: Zhonggao Gao and Wei Huang, E-mails: zggao@imm.ac.cn (Z. Gao) and huangwei@imm.ac.cn (W. Huang), Tel.: +86 10 63028096.

Received: 2016.07.14; Accepted: 2016.10.24; Published: 2017.01.01

Abstract

Phenylboronic acid (PBA)-mediated tumor targeting nanovector is an attractive strategy for enhancing siRNA delivery and treatment of metastatic cancers. However, its nonspecific binding with various biological membranes containing *cis*-diol moieties restricts its potential application by systematic administration. Herein, we constructed a novel pH-activated "sheddable" PEG-coated nanoparticle for effective treatment of primary tumors and metastases, which was based on the conjugation of catechol group modified poly(ethylene glycol) (PEG-Cat) and PBA-terminated polyethylenimine (PEI-PBA) via the borate ester formed between PBA and Cat. By virtue of the pH-dependent stability of borate ester in an aqueous medium, the PEG-shell could "shield" the PBA ligand in systemic circulation to reduce its "off-target effect", while PEG was detached at tumor extracellular pH (~6.5) to expose intact PBA moiety. Simultaneously, the PBA ligand could bind with overexpressed sialic acid residues on cancer cells, giving rise to enhanced cellular internalization. In addition, the PBA moieties could also couple with each 3'-end ribose of double-stranded siRNA. siRNAs were used as both a payload and a pH-responsive intermolecular cross-linker, and thereby acquired sufficient stability during circulating in blood and a rapidly triggered release in response to acidic endosomal/lysosomal pH-stimuli. As a result, this dual pH-sensitive nanoparticle showed enhanced siRNA uptake, gene silencing efficacy and anti-metastatic effects in vitro. Furthermore, in vivo studies demonstrated that PBA-based nanoparticles effectively accumulated in tumor and inhibited tumor growth and metastasis in 4T1 orthotopic mammary tumor model after intravenous administration.

Key words: Phenylboronic acid; pH-Responsive; Sialic acid targeting; Systemic siRNA delivery; Cancer Metastasis; Orthotopic breast murine model.

Introduction

Metastasis is the mainspring of breast carcinoma-related mortality among women worldwide[1]. During malignant transformation, tumor cells acquire a range of alterant characteristics enabling them to dissociate from tumors and metastasize to distant organs. Increased sialylated glycans on tumor cell surfaces is a specific characteristic related to advanced malignancy[2].

Increasing evidences have revealed that carcinomatosis-associated sialic acids (SA) over-expression on cell surface is confirmed in virtually each cancer type [3-5]. SA can help tumor cells escape recognition and elimination by the immune system, thus conducing to cancer metastasis. Aberrantly high SA expression of cell surface is emerging as a hallmark of cancer cell metastasis[5]. Therefore, targeting sialylated epitopes strategy provides a potent tool for metastatic cancer therapy.

Recently, phenylboronic acid (PBA)-functionalized polymers have been utilized for targeting SA residues on cancer cells[6-9]. PBA is a Lewis acid, able to form reversible borate esters with *cis*-diol-containing compounds including various carbohydrates [10, 11]. The highly binding capacity between PBA and SA, which even stable in mildly acidic environment[6], can facilitate tumor targeting, prolong the residence time in tumor sites and resist rapid washout from tumor tissues. This unique chemical characteristic provides advantageous bases for designing a PBA-mediated SA-targeting drug delivery system for cancer therapy. However, SA also exists on red blood cells or other components. Ligands for SA targeting should be inactive before reaching tumor sites[6]. To solve this issue, a "sheddable" strategy with a detachable PEG-shell is practical, which means that the outmost protective coating of PBA-based nanocarrier could be taken off upon access to the tumor microenvironment.

Small interfering RNA (siRNA) also offers a potent tool for metastatic breast cancer therapy [12]. Nonetheless, the systemic delivery of siRNA to target cells is still one of the main obstacles for successful gene silencing[13]. The important issue is to resolve the conflict between stabilizing the siRNA polyplex in systemic circulation and effectively release siRNAs upon reaching intracellular targets. Among multifarious efforts, the cross-linking strategy based on PBA-ribose interactions has been a sophisticated and promising solution[11]. As mentioned above, PBA could interact with carbohydrates including ribose of ribonucleic acids (RNAs) [10, 11]. Since a ribose ring exists at each 3′ end of double-stranded siRNA, this structural character entails not only a facile approach for siRNA to chemical conjugation with PBA moieties without any catalysts, but also plausible intermolecular cross-links via siRNA bridging, thereby further stabilizing the complex[11]. More importantly, the covalent phenylboronate esters are reversible by pH. They are thermodynamically stable at neutral or alkaline condition ($pH > pK_a$) but susceptible to acidity induced cleavage ($pH < pK_a$). Given pH decline in endosomes/lysosomes of tumor cells, the PBA-siRNA binding is spontaneous and reversible, which could be used to tailor the stability of complexes to realized controlled siRNA packing/unpacking to specific biological environment.

With all mentioned above in mind, a dual pH-responsive and tumor-specific nanovector was constructed to achieve cleavable PEGylation, targeted delivery and effective intracellular triggered-release of siRNA. The nanovector is consisted of α-methoxy ω-amino polyethylene glycol-catechol (mPEG-Cat) and PBA-grafted low molecular weight branched polyethylenimine (1,800 Da) (PEI-PBA). Here, catechol is an excellent *cis* diol-containing reagent to form complexes with boronic acids[14]. The spontaneous formation of boronate linkage between PBA and Cat allows facile attachment of mPEG-Cat onto PEI-PBA at neutral condition. Then, as illustrated in **Scheme 1**, the PBA-functional polymer (PEG-CPB-PEI) could condense siRNA into polyplex nanoparticles at pH 7.4 via a "synergetic assembly" approach of a facile PBA-ribose chemical binding and an electrostatic interaction generated from the cationic PEI with anionic phosphate group of siRNA. Once this combination was produced, a reversible equilibrium would shift to right to further promote the PBA-ribose binding (**Scheme S1**), thereby tightening the polyplex core and stabilizing the nanoparticles in physiological conditions. After intravenous administration the well-tailored nanoparticle preferentially accumulates in tumor by the enhanced permeability and retention (EPR) effect and avoids "off-target effect" with the protection of PEG corona. Subsequently, the PEG-shell is detached at tumor extracellular pH due to the unstable conjugation of PBA-catechol. And the exposed PBA moiety binds with over-expressed sialylated epitopes on cancer cells [5, 15], which accelerates the detachment of PEG and results in enhanced cellular internalization by virtue of both prolonged resident time on the cell surface and overexpressed SA receptor-mediated uptake. After internalization into the endosomes/lysosomes, the borate ester bond of PBA-ribose in the cross-linked core would be completely disrupted as the pH value further declines down to 4.5~5.5. Therefore, the nanostructure would entirely break down accompanied by rapid and triggered release of siRNA. Meanwhile, the PEI component promotes endosomal/lysosomal escape which allows siRNA to migrate into the cytoplasm for gene silencing.

In this work, the PEG-CPB-PEI (PCPP)/siRNA nanoparticle were prepared and well characterized in vitro and in vivo. Compared with other PBA-mediated tumor targeting nanovector for siRNA delivery[8, 9, 16, 17], the unique dual pH-responsive

architecture with functional versatility for siRNA delivery showed great advantages: (i) The introduction of an *ortho* aminomethyl group to boron decreased pK_a of boronic acid, which facilitated the PBA/*cis*-diols binding at neutral pH and stabilized nanoparticles during blood circulation. (ii) The PEG-shell on the surface of PBA-based polyplexes could "shield" the PBA ligand in systemic circulation to reduce its "off-target effect", while be detached at tumor extracellular pH to expose PBA, giving rise to enhanced cellular internalization. (iii) The acidity-labile conjugation of polymer-siRNA can tailor the cargo packing and unpacking in a pH-switchable manner, which resolved the conflict between stabilizing the siRNA polyplex in systemic circulation and effectively release siRNAs upon reaching intracellular targets. Therefore, this unique dual pH-sensitive and tumor-targeted nanoparticle showed enhanced siRNA uptake, gene silencing efficacy and anti-metastatic effects in vitro. More importantly, the survivin-targeted siRNA-loaded nanoparticles simultaneously suppressed the orthotopic tumor growth and spontaneous metastasis to liver or lung in 4T1 orthotopic murine model. We hope that this novel siRNA nanovector with pH-responsiveness and tumor-targeting ability holds great promise for cancer gene therapy.

Materials and Methods

Materials

Ethidium bromide (EtBr) and N-acetylneuraminic acid (Neu5Ac) were obtained from Sigma-Aldrich Inc. (Shanghai, China). The Cell Counting Kit-8 was purchased from DOJINDO Molecular Technologies, Inc. (Shanghai, China). 4',6-diamidino-2-phenylindole (DAPI) and Hoechst 33258 were bought from the Beyotime Institute of Biotechnology (Jiangsu, China). FITC-Annexin V/PI apoptosis detection kit was purchased from KeyGEN

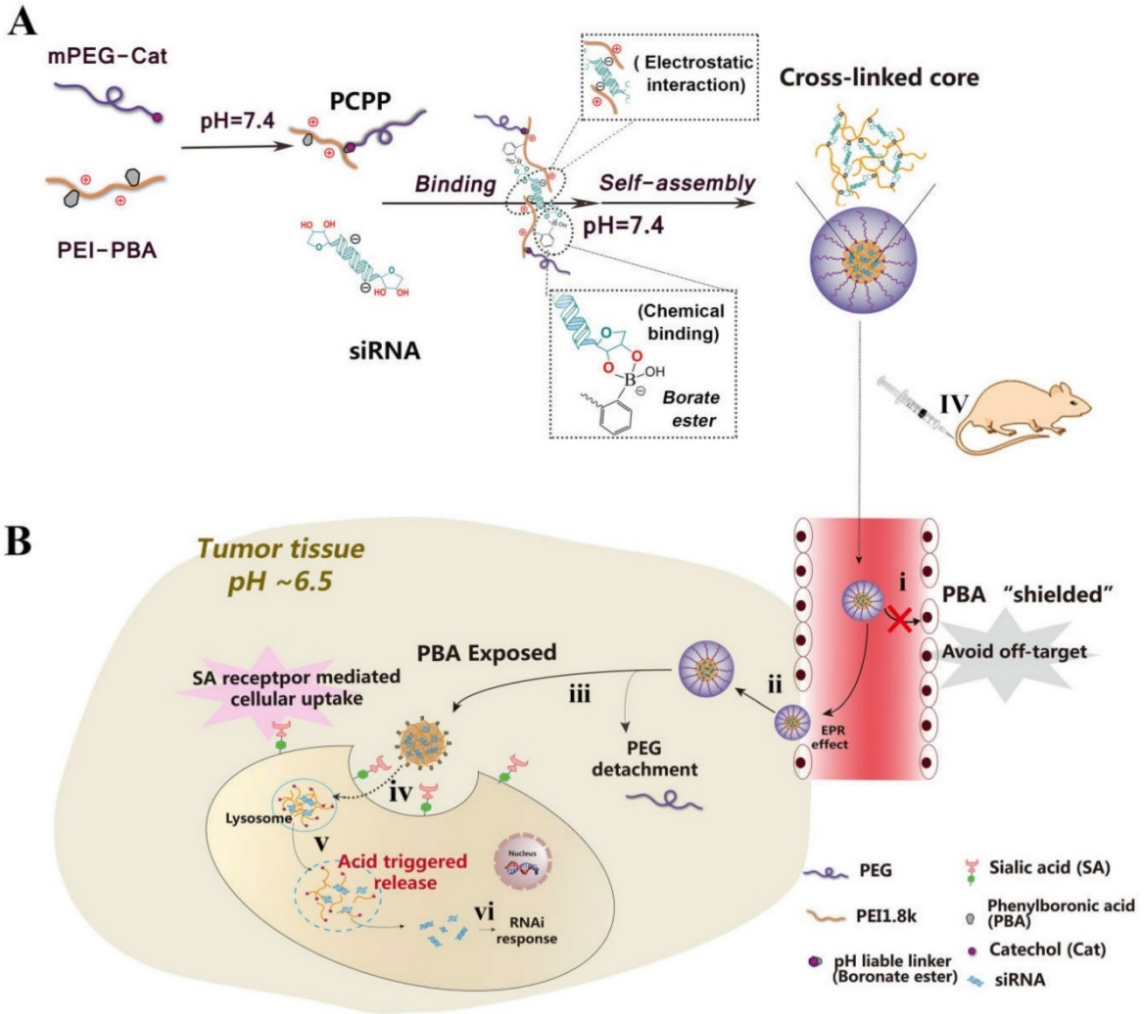

Scheme 1. (A) Schematic illustration for constructing PCPP/siRNA nanoparticles via a "synergetic assembly" approach of an electrostatic interaction and borate ester formation-mediated chemical binding. (B) Illustration of the dual pH-responsibility and tumor-targeted siRNA delivery by PCPP. (i) Avoiding "off-target" effect with the protection of PEG corona; (ii) Accumulation of PCPP/siRNA at the tumor site by EPR effect; (iii) Extracellular acidity-activated detachment of PEG-shell and exposure of PBA; (iv) PBA recognition and SA receptor-meditated cellular internalization; (v) Endosomal/lysosomal escape and acidity-triggered disassembly of nanoparticle accompanied by the release of siRNA; (vi) RNAi response induced by siRNA.

biosciences company (Nanjing, China). Matrigel and transwell chambers were bought from Corning (USA). Crystal violet staining solution was purchased from Solarbio (Beijing, China). Luciferase assay kit was from Promega Corporation (Fitchburg, WI, USA). In situ cell death detection kit-POD was supplied by Roche (Basel, Switzerland). Quant-iT™ RiboGreen® RNA Reagent and Kit was obtained from Thermo Fisher Scientific (Oregon, USA). FAM-siRNA, Cy3-siRNA and siRNAs of nonsense sequences (abbreviated as siN.C.) were purchased from GenePharma Co., Ltd. (Shanghai, China). Cy5-siRNA was supplied by Guangzhou RiboBio Co., Ltd. (Shenzhen, China). Anti-luciferase gene (siLuc: 5′-CUUACGCUGAGUACUUCGATT-3′) and anti-survivin gene (siSur: 5′-GCAUUCGUCCGGUUG CGCUTT-3′) were synthesized by GenePharma Co., Ltd. (Shanghai, China).

The 4T1 cell line was acquired from the Department of Pathology in the Institute of Medicinal Biotechnology at Peking Union Medical College, and cultured in RPMI 1640 medium supplemented with 10% FBS at 37°C in humidified atmosphere containing 5% CO_2.

Female BALB/c mice (6-8 weeks old) were acquired from Vital River Laboratory Animal Technology Co. Ltd. (Beijing, China). All animal experiments were carried out ethically approved by Laboratory Animal Ethics Committee in the Institute of Materia Medica in Peking Union Medical College. All experimental procedures were conformed with institutional guidelines and protocols for the care and use of laboratory animals.

Preparation and characterization of PCPP/siRNA nanoparticles

siRNA solution was mixed with PCPP solution in 10 mM HEPES buffer (pH 7.4) in equal volume at different N/P ratios. Then the mixed solution was vortexed for 30 s and incubated at room temperature for 20 min.

Size and zeta potential of PCPP/siRNA nanoparticles were measured using Malvern Zetasizer Nano ZS90 (Malvern Instruments Ltd., Worcestershire, UK). The morphology was investigated by transmission electron microscope (TEM).

pH-sensitive detachment of the PEG segment proved by ultraviolet spectroscopy and fluorescence quenching method

The phosphate buffer solution (pH 7.4/6.5/5.0) containing PCPP (1 mM) was examined by ultraviolet spectroscopy. Meanwhile, the mPEG-Cat and PEI-PBA were also analysed.

For fluorescence quenching assay, a PEI-PBA solution (15 mM) was mixed with the ARS solution (0.75mM) in phosphate buffer at pH 6.5. Then, the fluorescence intensity of PEI-PBA/ARS complex was measured after adding Neu5Ac of different concentrations by a fluorescence spectrometer (Fluorolog-Tau-3, ISA Co., Ltd., USA) (λ_{ex} 468 nm, λ_{em} 572nm). Neu5Ac is the most widely distributed SA. As a reference, the mixed solution of PEI-PBA and ARS at pH 7.4 was also detected.

In vitro release of siRNA

To investigate the release profile of siRNA in vitro, 100 μL of $PCPP_{siN.C.}$ nanoparticle dispersion containing 1.25 μM siRNA was suspended in PBS buffer (1 mL, pH 7.4/6.5/5.0) and shaked gently (100 rpm) at 37 °C. At predetermined time points, the samples were collected and centrifuged at 4°C, 15,000 ×g for 30 min. Then 100 μL of supernatant containing the released siRNA was mixed with a 200 times diluted RiboGreen reagent solution at a ratio of 1:1 (v/v). Fluorescence was measured by spectrofluorometry ($\lambda_{ex}/\lambda_{em}$: 480 nm/520 nm) and the amount of unencapsulated siRNA concentration was quantified by comparison to a standard curve. The equal amount of free siRNA was used as a reference.

Gel electrophoresis assay

The gel electrophoresis assays were conducted to investigate the condensing and protective ability of PCPP. Varying concentrations of PCPP were mixed respectively with 1 μg of siRNA at different N/P ratios ranging from 0 to 30. After mixing with 1μL 6 × loading buffer, the sample was electrophoresed on 4% agarose gel at 120 V for 20 min. Subsequently, the gel was stained with 0.5 mg/mL EtBr for 30 min and photographed under an UV image system (SIM135A, SIMON).

For RNA protection assay, naked siRNA and PCPP/siRNA nanoparticles were separately pretreated with RNase A for 0.5−12 h and incubated with heparin (20 mg mL^{-1}) for another 30 min. Finally, the samples were electrophoresed on 4% agarose gels as described above.

Heparin Displacement assay

For heparin displacement assay, the $PCPP_{siN.C.}$ nanoparticles were mixed with heparin sodium solution of different concentrations at pH 7.4 and 5.0, respectively. The $PEI1.8k_{siN.C.}$ and $PEI\text{-}PBA_{siN.C.}$ nanoparticles were employed for comparisons. Then after incubation at room temperature for 1 h, the released siRNA was calculated by RiboGreen® RNA method as previous description and the equal amount of free siRNA was used as a reference.

Confocal laser scanning microscopy (CLSM) analysis

4T1 cells were seeded onto coverslips in 24-well plates and cultured for 24 h. The next day, cells were treated with naked FAM-siRNA, PEI1.8k/FAM-siRNA or PCPP/FAM-siRNA for 4 h. For PCPP/FAM-siRNA, cells were incubated in pH 6.5 medium before nanoparticles were added. After washed with cold PBS, cells were fixed with 4% paraformaldehyde for 15 min. DAPI was subsequently added to stain the nuclei. Finally, the sample was observed and imaged on a confocal microscope (Carl Zeiss LSM 710, Carl Zeiss Microscopy GmbH, Germany). For endosomal/lysosomal escape investigation, cells were incubated with LysoTracker® Red DND-99 at 37 ℃ for 1 h before fixed with 4% paraformaldehyde.

To verify the sialic acid receptor-mediated cellular uptake, cells were incubated with sialidase (50 mU mL^{-1}) for overnight prior to addition of PCPP/Cy3-siRNA. The sialidase catalyzes the hydrolysis of SA residues from glycoproteins and oligasaccharides of cell surfaces. Then the cells were incubated with FITC-SNA, MAA or WGA (SNA 1μg mL^{-1}, MAA 5μg mL^{-1}, WGA 5μg mL^{-1}) for 30 min, followed by CLSM analysis to detect the SA on cell surfaces. And the intracellular uptake by normal cells was used as a control.

Flow cytometery analysis

4T1 cells were seeded in 12-well plates. After 24h incubation, FAM-siRNA-loaded nanoparticles in pH 6.5 or 7.4 medium were added and the cells were further cultured for 4 h at 37°C, followed by harvested with trypsin treatment. The collected cells were washed with PBS followed by centrifuged at 2,000 rpm at 4°C for 5 min in two cycles. Finally, the cells were resuspended with 500 μL PBS for analysis using a FACS Calibur flow cytometer (BD Biosciences, USA). To evaluate the hydrolysis effect of sialidase, the cells were incubated with sialidase and PCPP/Cy3-siRNA, as described earlier.

Knock-down of the endogenous reporter luciferase gene with $PCPP_{siLuc}$ nanoparticles

4T1-Luc cells, which stably express luciferase, were seeded into a 24-well plate. After 24 h proliferation, the cells were treated with serum-free medium. Subsequently, naked siLuc, $PEI1.8k_{siLuc}$, $PEI\text{-}PBA_{siLuc}$ and $PCPP_{siLuc}$ were added into wells. For $PCPP_{siLuc}$, cells were incubated in pH 6.5 medium before nanopaticles were added. the PBS and $lipofectamine\ 2000_{siLuc}$ lipoplexes were respectively used as negative and positive controls. After 4 hrs incubation and removing the old medium, fresh complete medium containing 10% FBS was added. Then at the end of culture time about another 44 h, the luciferase activity of cells per well was analyzed using luciferase assay kit. The luciferase gene silencing efficiency was calculated by Equation (1). To evaluate the influence of different pH values, the cells were treated with serum-free medium at different pHs (7.4 and 6.5), respectively.

$$\text{Luciferase gene silencing efficiency (\%)} = \frac{\text{luciferase activity}_{\text{control}} - \text{luciferase activity}_{\text{sample}}}{\text{luciferase activity}_{\text{control}}} \times 100 \quad \text{(Eq. 1)}$$

Proliferation inhibition assay

CCK-8 assay was conducted to study the proliferation inhibitory efficacy of $PCPP_{siSur}$ nanoparticles on tumor cells. 4T1 cells were seeded into a 96-well plate. After 24 h proliferation, cells were treated with naked siSur, $PEI1.8k_{siSur}$, $PCPP_{siSur}$ and $PCPP_{siN.C.}$ nanoparticles, respectively. The final siRNA concentration was 100 nM in each well. Then the procedure was performed in accordance with the reference[18], and the optical density (OD) was detected at 450 nm to calculate the cell viability according to Equation (S1). The cell viability with no treatment was served as 100%.

Wound healing assay

After 24 h-proliferation of 4T1 cells in 12-well plate, the confluent cell monolayer per well was wounded with a 200 μL pipette tip, washed with serum-free medium and exposed to $PCPP_{siSur}$ at the concentration of 100 nM siSur per well. Cells untreated and treated with naked siSur or $PEI1.8k_{siSur}$ were used as controls. Medium per well was replaced with fresh complete medium after 4 h incubation. The healing status of scratch wound were observed and imaged during the next culture time.

Transwell migration and invasion assay

For cell migration assay, 4T1 cells were seeded into a 6-well plate and pre-treated with naked siSur, $PEI1.8k_{siSur}$ and $PCPP_{siSur}$ (100 nM siRNA per well) for 24 h at 37℃, respectively. Then cells were collected, resuspended in serum-free RPMI 1640, and added into the upper transwell chambers. Simultaneously, the RPMI 1640 medium containing 10% FBS was served as a chemoattractant and added into the lower chambers. After incubation for 24 h, un-migrated cells from the upper side of the membrane were washed and removed. The migrated cells in the lower surface were fixed, stained with crystal violet and photographed in different view fields under a microscope. For quantitative assay, the crystal violet staining cells was dissolved in 33% acetic acid and their absorbance was measured at 570 nm. Results were normalized to the untreated 4T1 cells. Cell

invasion assay was conducted in the same manner but with a Matrigel-coated transwell chamber.

Cell Apoptosis Assay

4T1 cells were seeded into 12-well plates and cultured until adherence. Then cells were exposed to naked siSur, PEI1.8k$_{siSur}$ or PCPP$_{siSur}$ (100 nM per well) for 4 h, replaced with complete fresh medium and cultured for another 44 h. After washing with PBS, cells were fixed in 4% paraformaldehyde, stained with Hoechst 33258 (1 μg mL^{-1}) for 15 min and observed apoptotic nuclei using an inverted fluorescent microscope (IX51, Olympus, Japan). To quantitatively measure the amount of apoptotic cells, cells after treatments with different formulations were harvested by 0.25% trypsin without EDTA, washed twice with cold PBS, resuspended in binding buffer and stained with Annexin V-FITC/PI for 15 min at room temperature in the dark. Finally, the sample was analyzed using a FACS Calibur flow cytometer within 30 min.

In vivo tumor-targeting analysis by fluorescence imaging method

1×10^5 4T1 cells were orthotopically inoculated in the fourth mammary fat pad in the right lower abdomen of 6-8 weeks old female BALB/c mice. Tumor volumes were monitored with a vernier caliper every three day and calculated as [length× (width)^2]/2 after inoculation. When the tumor size reached around 500 mm^3, the BALB/c mice bearing tumors were randomly assigned into three groups (n=3) and administrated with PCPP$_{Cy5\text{-}siRNA}$, PEI1.8k$_{Cy5\text{-}siRNA}$ and naked Cy5-siRNA (Cy5-siRNA = 1.5 mg kg^{-1}) via the tail vain. Herein, naked Cy5-siRNA and PEI1.8k$_{Cy5\text{-}siRNA}$ were set as controls. The mice were anesthetized by continuous exposure to 2% isoflurane to keep sedation and fluorescence images were taken at different time intervals (3h, 6h and 24 h) using an in vivo imaging system (An IVIS® Spectrum CT in vivo imaging system, PerkinElmer, USA) (λ_{ex} = 538 nm and λ_{em} = 580 nm for Cy5-siRNA). After 24 h of injection, the mice were sacrificed and tissues such as tumor, liver, lung, heart, kidney and spleen were isolated for imaging. Finally, images were analyzed using Living Image software (version 4.4, Caliper Life Science, Inc. USA).

In vivo inhibition of tumor growth and metastasis

Female BALB/c mice (6-8 weeks old) bearing 4T1-Luc tumors were randomized into five groups (n=4) when the tumors reached around 80 mm^3. Then the mice were treated with saline, naked siSur, PEI1.8k$_{siSur}$, PCPP$_{siN.C}$ or PCPP$_{siSur}$ every 3 days for 6 times via tail vein administration. The dose of siRNA was fixed at 1 mg/kg. Meanwhile, the body weight of mice and tumor size were recorded. Moreover, the inhibition of primary tumor growth progression and anti-metastatic activity were evaluated by noninvasive bioluminescent imaging (BLI) on 4T1-Luc tumor bearing mice using in vivo imaging system. The mice were injected intraperitoneally with 100 μL D-luciferin (10 mg/mL) 10 min before BLI, followed by imaged under anesthesia. The radiance (ρ sec^{-1} cm^{-2} sr^{-1}) was calculated by measuring the photon flux at desired time points using Living Image software. In order to evaluate the antitumor efficacy, the tumor inhibition rate determined by the bioluminescent intensity could be calculated according to the following equation[19]:

$$\frac{I_c - I_d}{I_c} \times 100\% \qquad \text{(Eq. 2)}$$

where I_c is the bioluminescent intensity of the control group (the saline group), I_d is the bioluminescent intensity of naked siSur, PCPP$_{siN.C.}$, PEI1.8k$_{siSur}$ or PCPP$_{siSur}$ treated group.

On the 3rd day after the final treatment (Day 30 post-inoculation), all mice were sacrificed. Tumors were isolated to be weighed and measure apoptosis of the tumor cells was determined by terminal deoxynucleotidyl transferased dUTP nick end labeling (TUNEL) staining. The lung and liver were harvested from sacrificed mice. The metastatic nodules on lungs were photographed after fixed with Bouin's solution. The anti-metastatic efficacies after therapy were estimated by histological examination of lungs and livers using hematoxylin and eosin (H&E) staining method.

Statistical analysis

The results were expressed as mean ± standard deviation (S.D.). For analysis between two groups, student's t test was used to evaluate the statistical difference. Comparisons among multiple groups were performed by one-way analysis of variance (ANOVA) with Bonferroni's post hoc test. Statistical analysis was made using SPSS software, and *P* less than 0.05 was considered as statistically significant.

Results and Discussions

Preparation and characterization of the nanoparticles

In the study, mPEG-Cat, PEI-PBA and PEG-CPB-PEI (PCPP) were synthesized according to **Figure S1, S2** and **S3**. The synthesis procedures and characterization of polymers were detailed in the Supplementary Material. In the design of PCPP formation, the borate ester acted as a character of

"hinge" to spontaneously integrate mPEG-Cat and PBA-PEI into one entity via the conjugation of PBA and Cat, which could be readily formed in neutral aqueous medium without additional chemical agents. After mixing the two in HEPES buffer (pH 7.4) followed by dialysis against water, the PCPP polymer was lyophilized and stored at -20℃ for further use. It was worth mentioning that the introduction of an amine in *ortho*-position to the boronic acid in the chemical structure of PEI-PBA decreased pK_a of boronic acid, which facilitated higher association constants between PBA and *cis*-diols at neutral pH. (The details can be found in Supplementary Materials and the result was shown in **Figure S4A.)**

Then, the pH-responsive nanoparticles formed between PCPP and siRNA could be easily self-assemble at neutral pH in a facile manner via the combination of electrostatic interactions and PBA-ribose chemical binding (**Figure 1A**). After investigating the agarose gel electrophoresis, particle size and luciferase silencing efficiency on 4T1-Luc cells (data were not shown), the N/P ratio was optimized as 60 and the optimum ratio was chosen for further in vitro and in vivo researches. The nanoparticles exhibited a compact and spherical morphology (**Figure 1B**). The average size was 51.44 nm with a polydispersity index (PDI) of 0.196 (**Figure 1C**). The zeta potential of PCPP/siRNA was ~6 mV (**Figure 1D**). Compared with PEI-PBA/siRNA(~22.1 mV), the almost neutral zeta-potential at pH 7.4 suggested that the PCPP was successfully covered with a neutral PEG outer layer due to the borate linkage. Besides, the visible outmost layer of nanoparticles in TEM image (**Figure 1B(b)**) also indicated the PEG coating. **Figure 1E** presented the gel retardation results. As the N/P ratio between PCPP and siRNA increasing, the encapsulating ability of polymer raised, and complete condensation of siRNA could be achieved at N/P ratio of 15 or higher. To investigate the protective ability on siRNA from nuclease degradation, naked siRNA and PCPP/siRNA were separately incubated with RNase A for 30 min, and followed by gel electrophoresis assay (**Figure 1F**). Naked siRNA was quickly degraded by RNase A, whereas PCPP exhibited an sufficiently protective capability on siRNA against RNase A degradation.

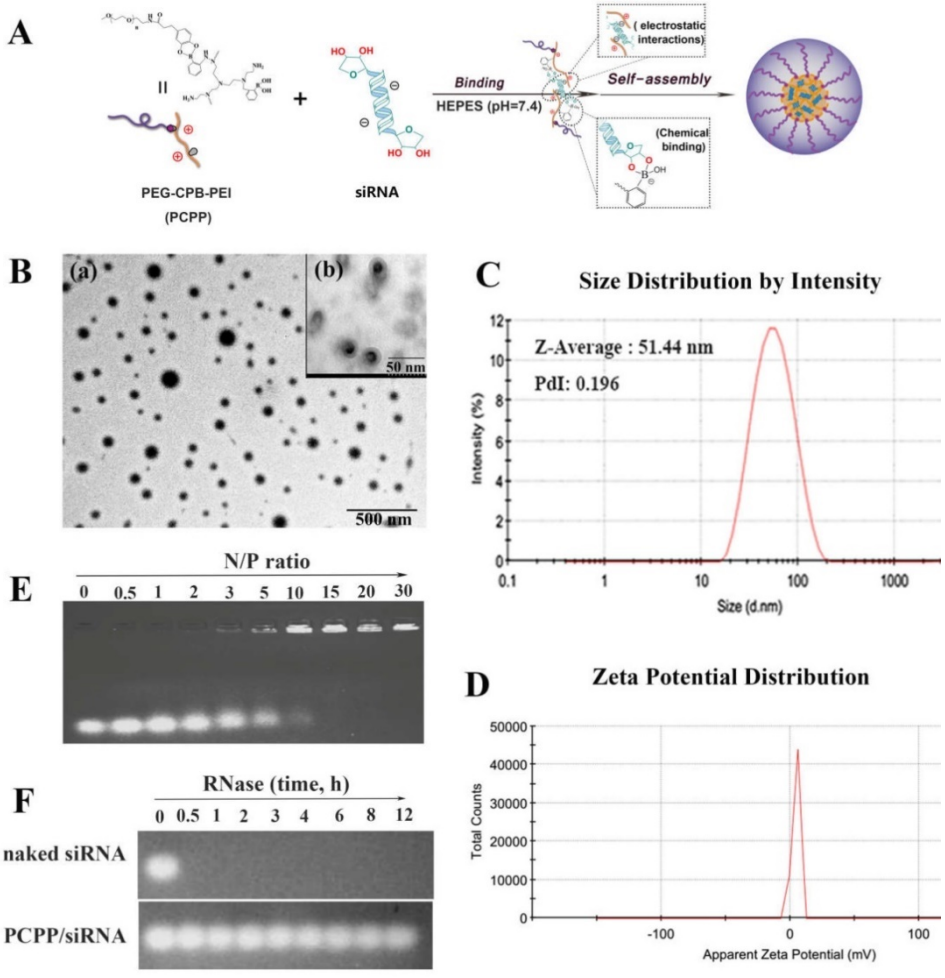

Figure 1. Characterization of the PCPP/siRNA nanoparticles. (A) The illustration for constructing PCPP/siRNA nanoparticles (B) Transmission electron microscopy (TEM) images. The scale bar represented 500 nm (a) and 50 nm (b). (C) Particle size distribution (intensity diameter). (D) Zeta potential distribution. (E) Gel electrophoresis assay for PCPP/siRNA binding capacity at different N/P ratios. (F) RNase A protection assay of PCPP/siRNA.

pH-responsive characterization of the PCPP polymer and siRNA-loaded nanoparticles

The acidity-lability of phenylboronate bond has been extensively studied[16, 20, 21]. In this work, the proof-to-concept experiment was first performed to verify the pH-dependent attachment/detachment of PEG segment. The PCPP polymer was dissolved in buffer solution and studied by ultraviolet spectroscopy under three conditions: pH 7.4, 6.5 and 5.0. As illustrated in **Figure 2A**, an absorption peak at 290 nm could be observed in UV spectra at pH 7.4, which clearly differed from the absorption of mPEG-Cat (280nm) and PEI-PBA (263 nm and 270 nm) (**Figure S8**). This new peak manifested the covalent formation of borate ester between PBA and catechol. However, the absorbance at 290 nm dramatically declined as the pH value of solution dropped to 6.5 or 5.0, indicating the dissociation of borate ester in acid environments. The above results revealed the pH-sensitive behavior of borate ester linkage and an acid-triggered invertible PEG coating for PCPP polymer. Moreover, this observation was well consistent with the fluorescence quenching results in **Figure 2B**, which elucidated the role of SA on the dissociation of PBA-catechol binding at pH 6.5. Here, we used Alizarin Red S (ARS) to replace mPEG-Cat, which both contained the same chemical group "catechol", to study the pH-dependent dissociation of PBA-catechol and the competitive relationship with SA. ARS is a catechol-containing dye, which could display dramatic color and fluorescent changes upon forming esters with boronic acid[22]. As displayed in Figure 2B, the fluorescence intensity of PBA-ARS was significantly decreased as the pH value declined from 7.4 to 6.5 without the addition of SA (I_0/I was 1.95 ± 0.25 when the concentration of Neu5Ac was zero). Then the fluorescence was quenched more strongly as the Neu5Ac concentration gradually increased. We have known that the catechol ligand and SA are both *cis*-diol-containing compounds. Therefore, the combination of PBA-SA would produce and accelerate the fluorescence quenching of PBA-ARS complex due to the competitive binding between PBA and diols.

To further confirm the PEG detachment and pH-sensitiveness of PCPP/siRNA nanoparticles, the zeta potential, particle size and release profile of siRNA were subsequently determined at different pHs. The zeta potential changes were initially investigated to check the PEG detachment (**Figure 2C**). As expected, with the decrease of pH value, zeta potential of PCPP/siRNA significantly rose up. Conversely, almost no change of zeta potential was obtained for PEI-PBA/siRNA polyplex after the same treatment. This phenomenon demonstrated the deshielding effect of the PEG shell at pH 6.5, which was triggered by the cleavage of PBA-catchol bonds. Next, we monitored the size variation by dynamic light scattering (DLS). As presented in **Figure 2D**, subtle alterations of the average diameter with narrowly distributed range were observed when the pH was maintained above 6.5. However, as the pH slumped to 5.0, sharp increments in both average size and PDI were obtained. A multimodal distribution with particles of 226.5 nm, 41.98 nm and 2.859 nm could be observed at pH 5.0, which indicated a dramatically structural transition of nanoparticles, probably leading to a rapid release of siRNA.

This concept was validated by the release behavior of siRNA in response to acidic stimulus. As shownd in **Figure 2E**, the cumulative release amount of siRNA significantly increased from 11.71% at pH 7.4 and 31.53% at pH 6.5 to 81.36% at pH 5.0 after 48 h incubation. Furthermore, the accelerated release of siRNA at pH 5.0 was remarkable within the first six hours compared with pH 6.5 or pH 7.4. These results indicated that by contrast with pH 7.4, the deshielding of PEG at pH 6.5 might destabilize the nanoparticle and facilitate the siRNA release after 48 h incubation, however, the loss of siRNA could be omitted within 6 hours since the substantial transfection should have happened in the first few hours. On the other hand, as the pH further declined to 5.0, the structure of nanoparticles was completely disintegrated, resulting in a rapid release of siRNA within such a short period. The pH-dependant manner of siRNA release provided fundamental evidences for acid-triggered structural evolution observed from the size changes, which was supported by similar findings in previous studies[23].

Stability of Nanoparticles Against Heparin Displacement

To investigate the stability of PCPP/siRNA against competing polyanions, the heparin displacement experiment was carried out with increasing amounts of heparin exposed to nanoparticles. Heparin is one of the negatively charged polysaccharides which is found in the interior of blood vessels, the extracellular matrix of many tissues and exists also on the cell surfaces[24]. It can disassemble the polymer/siRNA complex and lead to the release of siRNA. As shown in **Figure 2F**, almost 100% release of bound siRNA was obtained from unmodified PEI1.8k with a heparin concentration of 2.5 mg/mL at pH 7.4. By comparison, the release of siRNA was 56.52% and 76.32% respectively for PCPP and PEI-PBA under the same

condition. Not only sufficient siRNA protection from PCPP but also moderately improved stability for PEI-PBA could be acquired to resist the heparin replacement. This phenomenon indicated that the improved stability of PCPP/siRNA nanoparticle at pH 7.4 was attributed to the synergetic effect of the PEG shielding and the PBA-ribose binding compared with PEI1.8k. Nevertheless, the resistance to heparin displacement was decreased with increased acidity of the solution. The siRNAs were completely released more effectively at pH 5.0 with much lower heparin concentrations of 1.0 mg/mL and 0.8 mg/mL heparin for PCPP and PEI-PBA respectively. This phenomenon just supported the above results and explanations again: the detached PEG coating failed to protect nanoparticles against heparin displacement at pH 5.0, and on the other hand the disassociation of PBA-ribose binding led to a structural change of nanoparticle in such an acidic circumstance. Therefore, the PCPP polymer had much less binding affinity with siRNA, resulting in an effective release of siRNA in endosomal or lysosomal condition. As we known, for successful RNAi-based therapy via systematic administration, it is vital to optimize the polymer/siRNA stability in circulation and an effective siRNA release in cytoplasm. Obviously, PCPP could meet the demand and have promising potential for in vivo application.

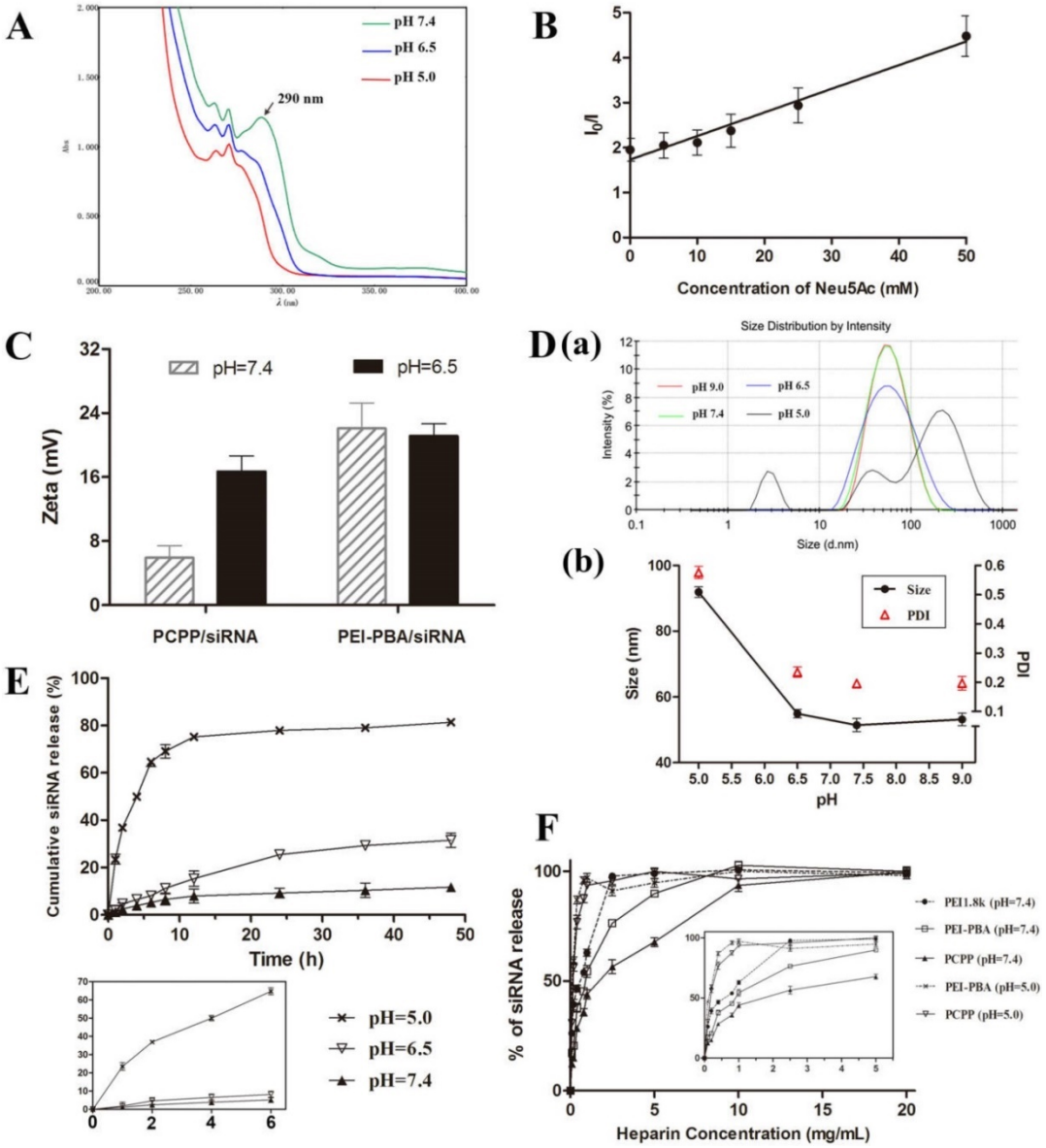

Figure 2. pH-Responsibility of PCPP and siRNA-loaded nanoparticles. (A) UV-absorption spectra of PCPP at different pHs. (B) The fluorescence of ARS/PEI-PBA in PBS buffer at pH 6.5 was measured in the presence of Neu5Ac at various concentrations. I_0 represents the fluorescence intensity of ARS/PEI-PBA at pH 7.4 without Neu5Ac and I represents the fluorescence intensity of ARS/PEI-PBA at pH 6.5 after adding different concentrations of Neu5Ac. (C) Zeta potentials of PCPP/siRNA and PEI-PBA/siRNA at pH 7.4 and 6.5. (D) Size distribution graph (a) and variation of particle size and PDI (b) at different pH values. (E) Cumulative siRNA release from PCPP/siRNA nanoparticls in different acidic conditions (n=3). The main graph shows the whole release profiles in 48 h, while the small chart in the lower-left corner magnifies the first 6 h portion; (F) Heparin displacement assay for different siRNA-loaded nanoparticles. The main graph shows the stability of nanoparticles challenged with increasing concentrations of heparin, and the small graph within magnifies the low concentrations of heparin (0-5 mg/mL) for easy observation.

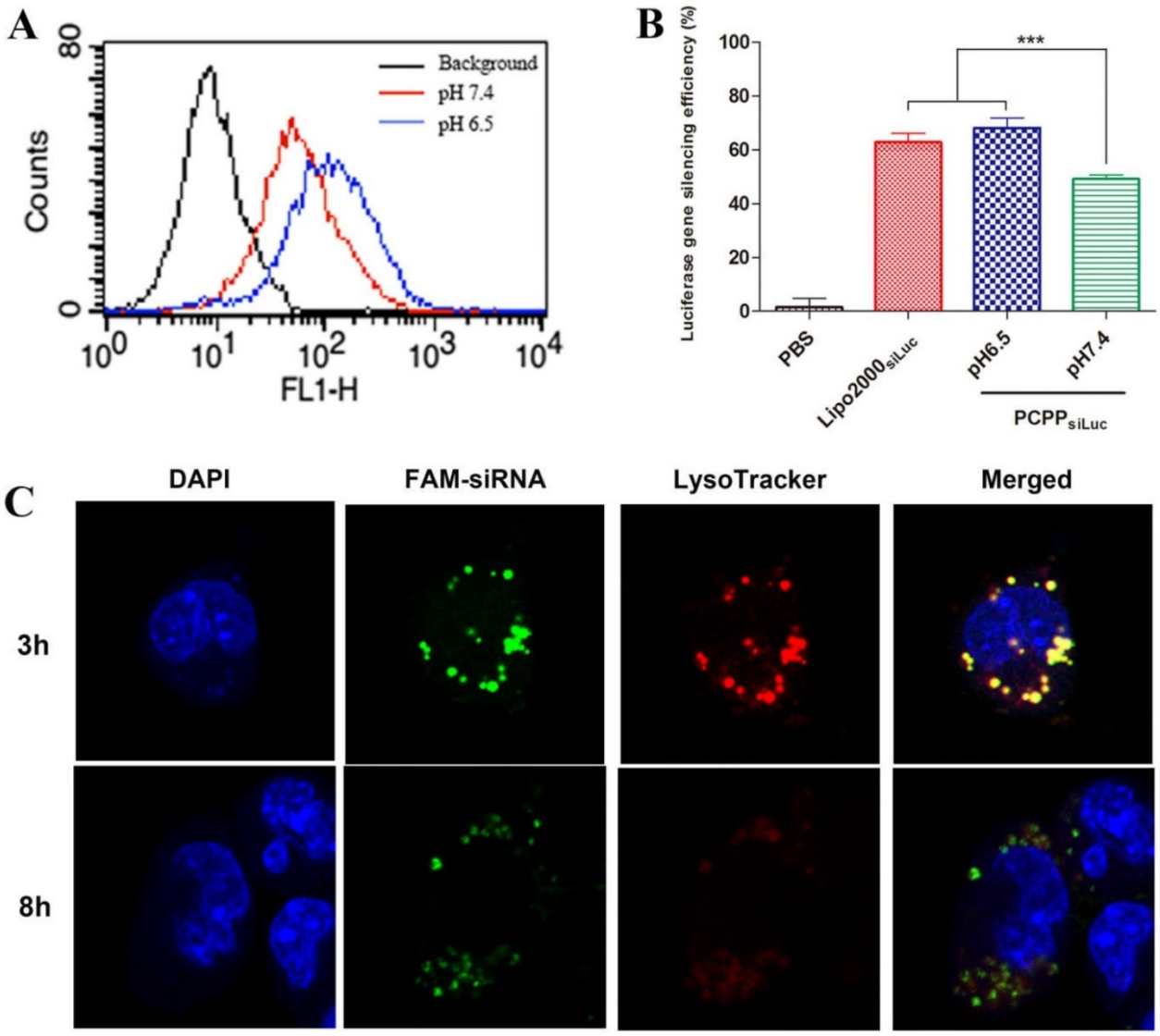

Figure 3. (A) Cellular uptake of PCPP/FAM-siRNA nanoparticles at pH 7.4 (red profile) or 6.5 (blue profile) by flow cytometry analysis on 4T1 cells. (B) Luciferase gene silencing of $PCPP_{siLuc}$ nanoparticles on 4T1-Luc cells at different pH values. (n = 3, ***$P < 0.001$). (C) Intracellular biodistribution of PCPP/FAM-siRNA nanoparticles in 4T1 cells. The DAPI (blue) and LysoTracker® Red DND-99 (red) were used for staining nucleus and endosomes/lysosomes, respectively.

Extracellular pH triggered cellular uptake and enhanced gene silencing effects of PCPP/siRNA nanoparticles in vitro

Efficient cellular uptake is vital in siRNA delivery. In view of the pH-responsive ability of PCPP, we investigated the cellular uptake of PCPP/FAM-siRNA at different pHs. 4T1 cells were treated with PCPP/FAM-siRNA at pH 6.5 or 7.4 for 4 h, and the intracellular fluorescence intensity was detected with flow cytometry. As shown in **Figure 3A**, in comparison with blank cells without treatment (black profile), highly fluorescent intensities were observed within cells transfected by PCPP/FAM-siRNA at pH 7.4 (red profile) or pH 6.5 (blue profile) indicating that the nanoparticles were effectively uptaken by cells. Furthermore, much more efficient cellular uptake was observed at pH 6.5, suggesting that siRNA accumulation was increased in 4T1 cells because covered PEG corona could be readily detached from the outer layer of the nanoparticles at pH 6.5. Therefore, it is reasonable to consider that the effective entry into cells and siRNA release into the cytoplasm of PCPP/siRNA was subsequently accompanied by enhanced gene silencing. Accordingly, the luciferase gene silencing ability of $PCPP_{siLuc}$ nanoparticles were perfomed on 4T1-Luc cells at different pH values. Here, the endogenous reporter gene of luciferase in 4T1-Luc cells acted as a silenced target by siLuc. The PBS and Lipofectamine 2000_{siLuc} complexes respectively served as negative and positive controls. The result was shown in **Figure 3B**. Down-regulation of the luciferase expression in a pH-dependent manner was

also obtained in the $PCPP_{siLuc}$ group, and it was more effective at pH 6.5 than at pH7.4 ($P < 0.001$). From these data, we concluded that profiting from the detachment of PEG at pH 6.5 and PBA-SA binding, enhanced cellular uptake of $PCPP_{siLuc}$ nanoparticles was realized accompanied by increasing gene silencing efficiency.

Endosomal/lysosomal escape

After internalization of PCPP/siRNA nanoparticles, endosomal/lysosomal escape was a key step for subsequent gene silencing. In our work, the acidification of endosomes/lysosomes would expedite the dissociation of pH-responsive nanostructure and facilitated siRNA release into cytoplasm (**Figure 3C**). After cells incubated with PCPP/FAM-siRNA for 3 h, the green fluorescence of FAM-siRNA was primarily found to be co-localization with the red signal of LysoTracker, indicating effective intracellular uptake and endosomal/lysosomal entrapment of PCPP/siRNA. However, separated fluorescence signals of FAM-siRNA and LysoTracker were observed after 8 h incubation, implying efficient endosomal/lysosomal escape of nanoparticles.

In vitro targeting ability of the nanoparticles

Aberrantly high sialylated glycoprotein in cancer cells is considered as a distinctive characteristic related with malignant levels and a hallmark of tumor metastasis[25]. SA are usually detected in the non-reducing terminatio of glycoproteins and glycolipids mainly via a α2,3- or α2,6- linkage to galactose (Gal), galactosamine or N-acetylgalactosamine (GalNAc) besides α2,8- linked to N-acetylneuraminic acid[26]. PBA is a potent tumor-targeting ligand, which could bind with the overexpressed SA in tumor cells. Here, the binding ability of PCPP with sialylated epitopes in 4T1 cell was conducted in vitro.

Firstly, the cellular uptake of PCPP/FAM-siRNA were investigated by confocal laser microscopy. As controls, naked siRNA and PEI1.8k/FAM-siRNA (without PBA) were used. As illustrated in **Figure 4A**, after incubating cells with different formulations, the intracellular fluorescent intensity of PCPP/FAM-siRNA was notably greater than that of naked siRNA or PEI1.8k/FAM-siRNA. Consistent results were acquired by flow cytometry analysis (**Figure 4B**). In comparison with naked FAM-siRNA (blue profile) and PEI1.8k/FAM-siRNA (green profile), the intracellular fluorescence intensity in PCPP/FAM-siRNA group (red profile) was significantly higher ($P < 0.001$), which indicated that PCPP/siRNA could be uptaken by 4T1 cells more effectively, thus resulting in much stronger gene silencing ability of $PCPP_{siLuc}$ compared to $PEI1.8k_{siLuc}$ due to specific affinity of PBA with cells (**Figure 4C**).

Afterwards, in order to verify the enhanced internalization of PCPP/siRNA via the SA receptor-mediated uptake, we studied the effect of sialidase on the cellular uptake of nanoparticles. Results of flow cytometry assay (**Figure S7**) firstly demonstrated the declined expression of SA after cells were incubated with sialidase overnight (The details were described in Supplementary Material). Then, the cellular uptake of nanoparticles was investigated after 4T1 cell were pre-treated with sialidase before incubation with PCPP/Cy3-siRNA nanoparticles. As illustrated in **Figure 4D**, compared to normal cells (without sialidase treatment), decreased green fluorescence intensities of FITC were observed in sialidase-treated cells, implying the weak SA expression on cell membranes. In line with these findings, drastically decreased intracellular red fluorescence signal of Cy3-siRNA was observed after treatment with PCPP/Cy3-siRNA. Whereas, a strong red fluorescence intensity was still shown inside normal cells. Moreover, the quantitative result by flow cytometry assay confirmed that after sialidase treatment, cellular uptake of PCPP/Cy3-siRNA was significantly reduced (**Figure 4E**).

In summary, not only could PCPP/siRNA improve the cellular uptake and gene silencing (compared to nanovector without PBA), but also pre-treating cells with sialidase resulted in dramatically poor cellular uptake. These results demonstrated the specific binding ability of PCPP with SA on cell surfaces.

Proliferation inhibition and inducing apoptosis effects of $PCPP_{siSur}$ nanoparticles in vitro

Survivin, a unique anti-apoptosis gene, is found over-expressed in breast carcinoma and highly associated with the metastasis of mammary tumor cells[27]. Owing to its importance in tumorigenesis, we first investigated the proliferation inhibitory capability of $PCPP_{siSur}$ on 4T1 cells. As illustrated in **Figure 5A**, the cell viability in $PCPP_{siSur}$ group (34.3±4.3%) was sharply lower than that of naked siSur (92.1±2.2%) and $PEI1.8k_{siSur}$ (85.0±2.4%) ($P < 0.001$).

Since survivin is a powerful inhibitor of programmed cell death (apoptosis)[27], cell apoptosis experiments were performed to reveal whether the above mentioned anti-proliferation of $PCPP_{siSur}$ was achieved by inducing apoptosis. Firstly, apoptotic nuclei of 4T1 cells was observed after staining by Hoechst 33258 under a fluorescence microscopy (**Figure 5B**). Cells, which had fluorescent brightly blue

nuclei and apoptotic bodies containing chromatin fragments, were generally deemed as apoptotic cells[28]. As indicated in Figure 5B, 4T1 cells treated with naked siRNA displayed no apoptosis features and some degree of apoptotic nuclei could be observed in PEI1.8k$_{siSur}$ group. However, the apoptotic effect significantly increased in PCPP$_{siSur}$ group. Chromatin condensation and nuclear fragmentation were typically observed in cells after treated with PCPP$_{siSur}$ for 48 h. The apoptotic cells were further quantified by flow cytometric analysis with Annexin V-FITC/PI staining (**Figure 5C**). After 24 h transfection, 57.06% of apoptotic cells occurred in the PCPP$_{siSur}$ group, whereas, the percentages in the groups of naked siRNA and PEI1.8k$_{siSur}$ were 5.12% and 7.36%, respectively.

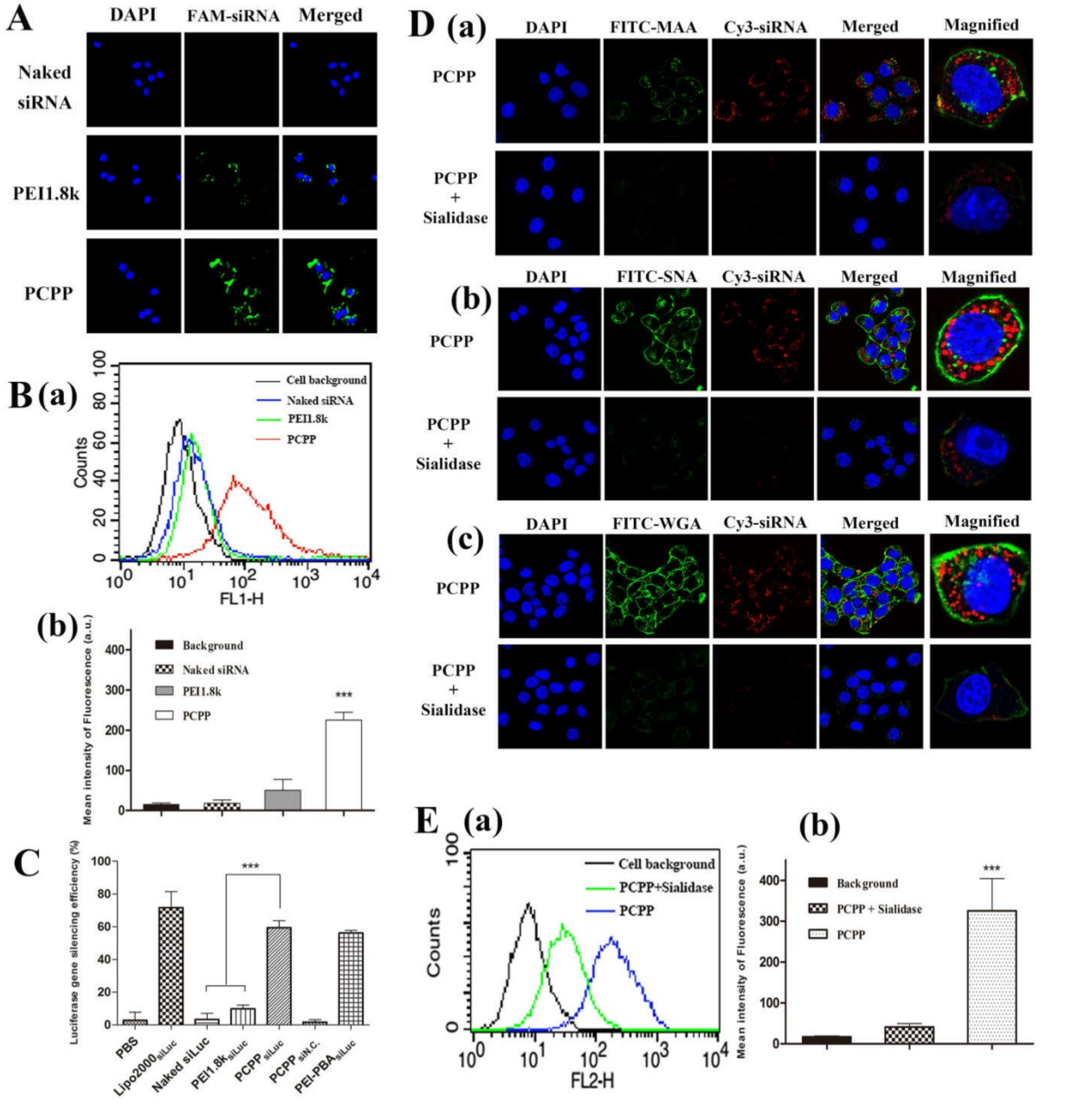

Figure 4. In vitro targeting ability of the nanoparticles. Cellular uptake of naked FAM-siRNA, PEI1.8k/FAM-siRNA and PCPP/FAM-siRNA nanoparticles by CLSM (A) and flow cytometry analysis (B). Representative diagram (B-a) and quantification of the flow cytometry analysis (n = 3) (B-b) is shown. (C) Luciferase gene silencing of different nanoparticles on 4T1-Luc cells. (n = 3). After treatment with sialidase, the cellular uptake of PCPP/Cy3-siRNA in 4T1 cells was analyzed by CLSM (D) and flow cytometry assay (E). To hydrolyze specifically SA, 4T1 cells were pre-treated with sialidase before incubation with PCPP/Cy3-siRNA and then incubated with FITC-MAA (D-a), SNA (D-b) or WGA(D-c) to detect the SA expression on cell surface. Representative flow cytometry analysis showing relatively reduced uptake after treatment with sialidase (E-a), and the mean fluorescence intensity in the cells was then calculated (n = 3) (E-b). (*** $P < 0.001$).

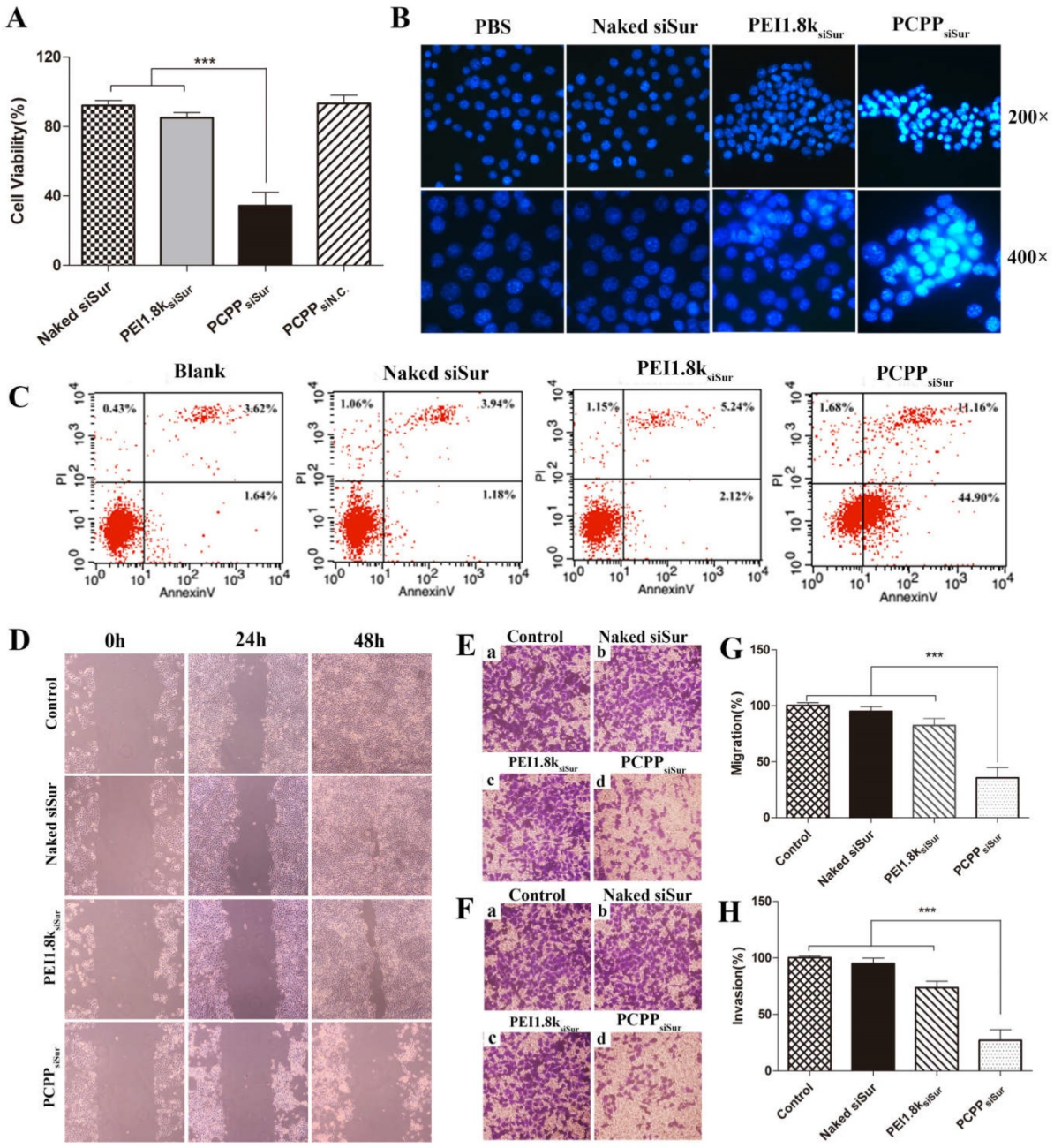

Figure 5. (A) Proliferation inhibition assay of siSur-loaded nanoparticles in 4T1 cells (n=6). (B) Representative image of nuclei morphological changes by staining with Hoechst 33258 after cells exposed to PBS, naked siSur, PEI1.8k$_{siSur}$ or PCPP$_{siSur}$. (C) Quantitative detection of apoptotic 4T1 cells induced by different formulations. (D) Wound healing images after scratch for 24 h and 48 h. Cells with no treatment were used as control. Representative 100× microscopy images of migration (E) and invasion (F) of 4T1 cells after treated with naked siSur (b), PEI1.8k$_{siSur}$ (c) or PCPP$_{siSur}$ (d) in transwell assay. Cells with no treatment were used as control (a). Quantitative cell migration (G) and invasion (H) were evaluated by measuring the dissolved crystal violet in 33% acetic acid at 570 nm. (n = 3, *** P <0.001).

In vitro cell migration and invasion experiments

The anti-metastatic effects of PCPP$_{siSur}$ in vitro were assessed with the cell migration and invasion evaluations. First of all, wound healing assay was carried out to study the inhibitory effect of naked siSur, PEI1.8k$_{siSur}$ and PCPP$_{siSur}$ on cell motility. As illustrated in **Figure 5D**, the wound in blank control group was almost completely healed, indicating a superior metastatic property of 4T1 cells. In the naked siSur and PEI1.8k$_{siSur}$ group, the wound get narrow and almost invisible after 48 h incubation. However, no obvious change was observed in the PCPP$_{siSur}$ group. Then, the transwell assays were conducted to further study the inhibitory effect of longitudinal motility and invasion ability on 4T1 cells. The results were presented in **Figure 5E-H**. Cells in the blank control group crossed the membrane and covered almost the entire lower surface (**Figure 5E (a), F (a), G, H**), which illustrated the strong migratory and

invasive ability of 4T1 cells. Naked siSur displayed no inhibitory ability (**Figure 5E (b), F (b), G, H**). PEI1.8k$_{siSur}$ to some degree showed inhibitory capacity on migration and invasion with the percentage of 82.4±6.4% and 73.7±5.6% on covering lower surface (**Figure 5E (c), F (c), G, H**). Notably, the migratory and invasive capacities of 4T1 cells were sharply suppressed after PCPP$_{siSur}$ treatment, with the migratory and invasive rates of 35.7±9.3% and 27.1±8.9%, respectively (**Figure 5E (d), F (d), G, H**). Taken together, the above data suggested that PCPP$_{siSur}$ exhibited great potential in anti-metastatic effects on 4T1 cells.

In vivo tumor accumulation and biodistribution

Real-time in vivo fluorescence imaging was used to investigate the targeting ability of PCPP/Cy5-siRNA in female BALB/c mice bearing 4T1 primary tumor xenografts. As depicted in **Figure 6A**, much higher fluorescence intensity was visualized at primary tumor sites in the PCPP$_{Cy5\text{-}siRNA}$ group compared with PEI1.8k$_{Cy5\text{-}siRNA}$ and naked Cy5-siRNA groups. Furthermore, the intensity of the signal was still strong at 24 h post-injection, revealing that PCPP/Cy5-siRNA nanoparticles accumulated effectively in tumors. Then 24 h later, mice were sacrificed and the total fluorescence intensity in major organs from each group were collected and quantitatively analyzed (**Figure 6B and 6C**). As a result, PCPP$_{Cy5\text{-}siRNA}$ accumulated in tumor significantly higher than other two groups ($P < 0.001$). Besides, the fluorescence intensity in all the dissected organs of PCPP/Cy5-siRNA group was much higher than that of PEI1.8k/Cy5-siRNA group. This could be attributed to the higher stability of PCPP/Cy5-siRNA nanoparticles, thereby helping to prolong the circulation half-life and facilitate accumulation in tissues.

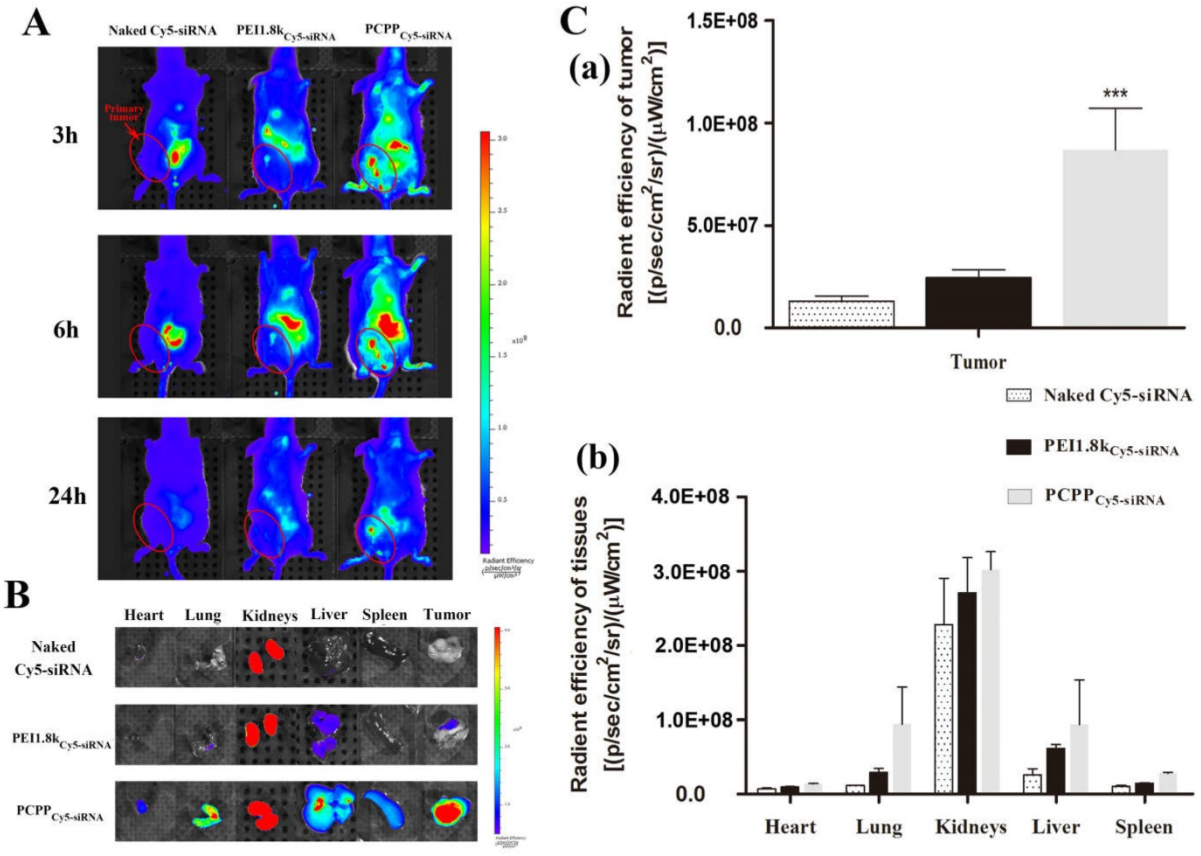

Figure 6. (A) In vivo fluorescent images of 4T1 tumor bearing mice treated with different Cy5-siRNA loaded nanoparticles (equivalent Cy5-siRNA, 1.5 mg/kg) via tail vein injection. Images were taken at 3 h, 6 h and 24 h after injection. Fluorescent images (B) and quantitative analysis (C) of isolated tumor masses (C-a) and major organs (C-b) at 24 h post-injection. (n = 3, *** P <0.001).

The biodistribution characteristic of drug is an important element determining its therapeutic effect, thus is regarded as an vital property of the nanocarrier[29, 30]. Usually, size and surface property are two vital factors affecting the delivery efficiency of nanocarriers[31]. The high tumor targeting ability of PCPP might benefit from the reasons below: Firstly, the size of PCPP/siRNA was within the appropriate range (10-100 nm), which escaped clearance from blood circulation by extravasation or kidney (less than 10 nm)[32] and facilitated accumulation within tumors by the EPR effect (less than 100 nm)[33]. Secondly, intermolecular cross-links between PBA and siRNA improved the structure stability of nanoparticles and therefore helped to enhance the tumor accumulations; Third, systemic circulation was prolonged as a result of the PEG presence[32, 34], nonetheless, after extravasation from capillaries into the tumor sites, PEG-shell can be detached at a low extracellular pH. Moreover, because of the high affinity between PBA and SA, PCPP/siRNA nanoparticles can bind to cells, followed by prolonged retention time in tumor, SA receptor-mediated uptake and markedly increased internalization into cells. The real-time in vivo fluorescence imaging demonstrated once again that PCPP/siRNA nanoparticles accumulated more effectively in the 4T1 tumors because of not only passive but also active targeting effects**.**

In vivo primary tumor inhibition by inducing apoptosis effects

To confirm the in vivo anti-tumor efficacy, 4T1 tumor-bearing mice were devided into five groups and treated with saline, naked siSur, PEI1.8k$_{siSur}$, PCPP$_{siN.C}$ and PCPP$_{siSur}$ separately. The body weights and tumor volumes were measured every three days until 30 days. When the experiment was over, tumors were separated, weighted and photographed. As presented in **Figure 7**, PCPP$_{siSur}$ exhibited the best inhibitory efficiency in tumor growth by comparison with other groups. The results of tumor growth curves (**Figure 7A**) displayed that tumors in naked siSur and PEI1.8k$_{siSur}$ groups both grew quickly. Compared with the saline group, no remarkable differences were shown among the three groups, suggesting that both naked siSur and PEI1.8k$_{siSur}$ could not suppress the tumor growth. The tumor growth of mice in PCPP$_{siSur}$ group exhibited a relatively gradual profile and the smallest volume (**Figure 7A and C**), suggesting that PCPP$_{siSur}$ nanoparticles effectively inhibited the tumor growth in vivo. Moreover, the tumor volume profile of mice in PCPP$_{siN.C.}$ group was almost overlapped with the saline group, indicating that there was no anti-tumor effect of the biomaterial PCPP itself. On the 3rd day after the final treatment (days 30 post-inoculation), all mice were sacrificed. Tumors were separated to measure the weight and apoptosis of the tumor cells was determined by TUNEL staining. As shown in **Figure 7D**, the average tumor weights of mice receiving PCPP$_{siSur}$ were noticely less than that of mice treating with naked siSur, PEI1.8k$_{siSur}$, PCPP$_{siN.C}$ control and the saline control (P < 0.001). The body weights of mice in all groups displayed no obvious loss (**Figure 7B**), indicating no terrible systemic toxicity of nanoparticles.

For the purpose of explaining the tumor inhibitory effect from the viewpoint of cells, the tumors were further investigated with TUNEL assay for analysis of apoptosis. Representative fields of view from each group were shown in **Figure 7E**. As compared to other groups, mice treated with PCPP$_{siSur}$ nanoparticles displayed higher rate of apoptosis in accordance with the anti-tumor results. As we known, TUNEL staining was characterized for apoptosis. This result was in line with the inducing apoptosis effects in vitro, which confirmed that the enhanced anti-cancer effect of PCPP$_{siSur}$ nanoparticles was attributed to inducing cell apoptosis.

In vivo anti-metastasis effect

In this study, we employed in vivo bioluminescence imaging followed by post-mortem dissection to investegate the anti-metastatic abilities of PCPP$_{siSur}$ in 4T1-Luc tumor-bearing mice. First, 4T1-Luc cells expressed luciferase were inoculated at the fourth mammary fat pad of female BALB/c mice. Bioluminescence imaging was utilized to monitor tumor growth in situ and the metastasis foci in order to evaluate the tumor inhibition and anti-metastatic efficacies of agents[35, 36] (**Figure 8A**). As shown in Figure 8A, the bioluminescent images were acquired on day 14, 20 and 30 post-inoculation and the bioluminescent intensity of primary tumor was calculated using Living Image software. The bioluminescence level correlated with the cancer burden[36]. Although bioluminescence signals of the mice in all groups showed linear increase over tumor inoculation time, the tumor growth in PCPP$_{siSur}$ group showed a significantly slow increase. Compared with the saline treated group, the tumor inhibition rates of naked siSur, PEI1.8k$_{siSur}$ and PCPP$_{siSur}$ were 0.93±1.25%, 5.56±1.75% and 61.6±0.93%, respectively as determined by Equation (2) according to the abdominal bioluminescent intensity of tumor-bearing mice on Day 30 (P < 0.001; **Figure 8B**). This result revealed that PCPP$_{siSur}$ could effectively inhibit tumor growth compared with naked siSur and PEI1.8k$_{siSur}$, which was in coincidence with the above results of

primary tumor inhibition experiment. Also as depicted in Figure 8A, on day 30 post-inoculation bioluminescence signals in the thoracic region became apparent in mice from the saline, naked siSur, $PCPP_{siN.C.}$ and $PEI1.8k_{siSur}$ groups, which meant metastasis occurred in the above groups although micro metastasis have probably seeded earlier[35, 37, 38]. To demonstrate the results in Figure 8A, white metastatic nodules on lung were obvious after immersing lungs in Bouin's fixative for 24 h. The amount and size of metastasis nodules were taken as indicators of tumor cell colonization in the lungs. The results were illustrated in **Figure 9A-F**. Compared with saline group (Figure 9B), the number of metastatic nodules in lungs of naked siSur (Figure 9C), $PCPP_{siN.C}$ (Figure 9D) and $PEI1.8k_{siSur}$ groups (Figure 9E) displayed similar degree of tumor burden. However, similarity of lung surface was found in normal mice (Figure 9A) and the $PCPP_{siSur}$ group (Figure 9F), reflecting that mice in $PCPP_{siSur}$ group did not go through lung metastasis. The H&E staining results further verified that there were no metastatic foci in lung and liver of mice treated with $PCPP_{siSur}$ (Figure 9L and 9R). The lung structure and alveolar septum as well as hepatic cells in the mice of $PCPP_{siSur}$ group were almost as the same as those of normal mice (Figure 9G and 9M). This indicated that $PCPP_{siSur}$ had obvious effect on suppressing the hepatic and pulmonary metastasis of 4T1-tumor.

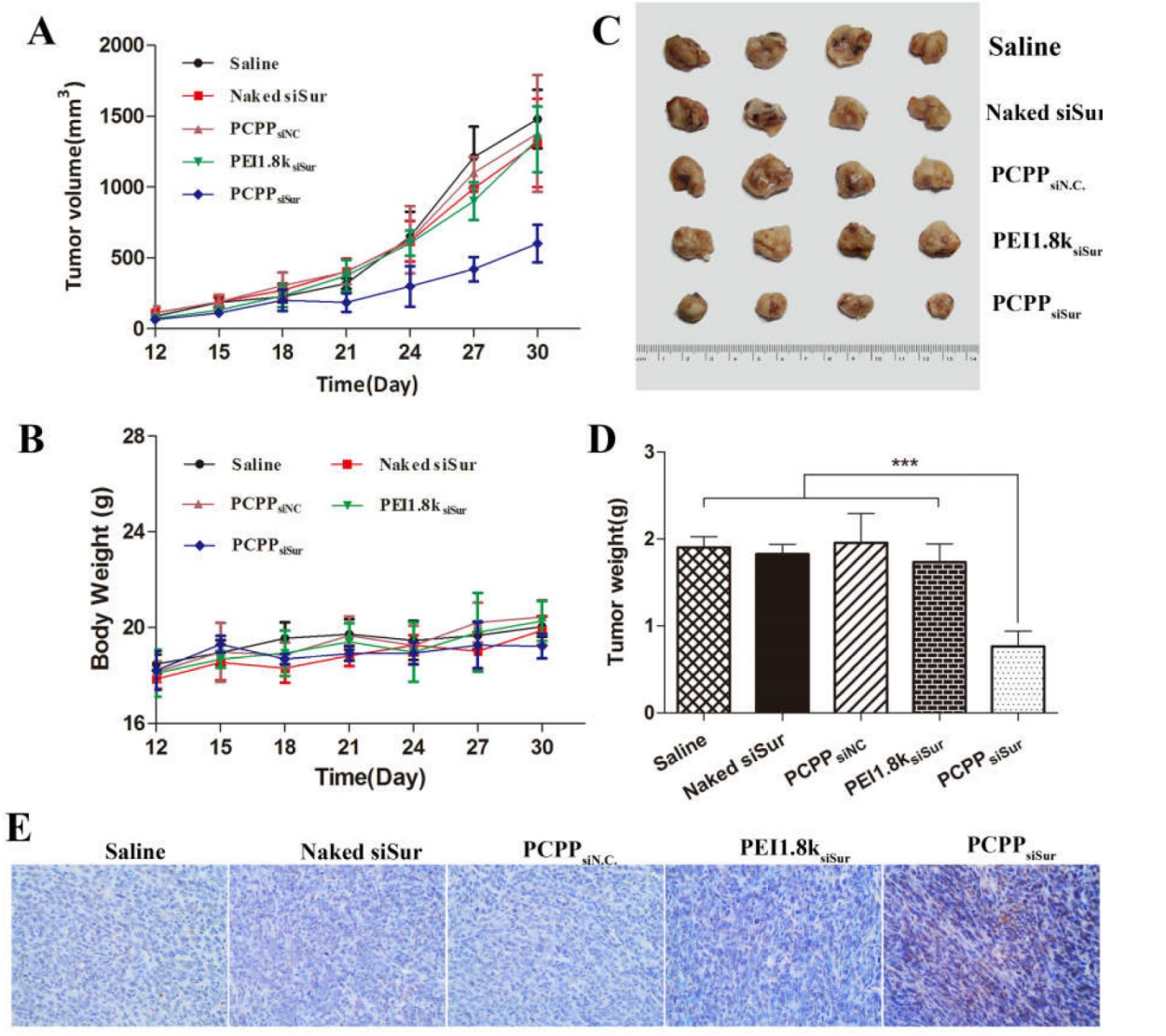

Figure 7. In vivo anti-tumor activity of different siSur-loaded nanoparticles on 4T1-Luc tumor bearing mice. The changes of tumor volume (A) and body weight of mice (B) measured every 3 day for 30 days. The tumor photos (C), tumor weights (D) and representative image for TUNEL assay (representative 200× microscopy images) (E) of 4T1-Luc tumor on Day 30 (n=4). The brown staining in TUNEL assay represents apoptotic cells.

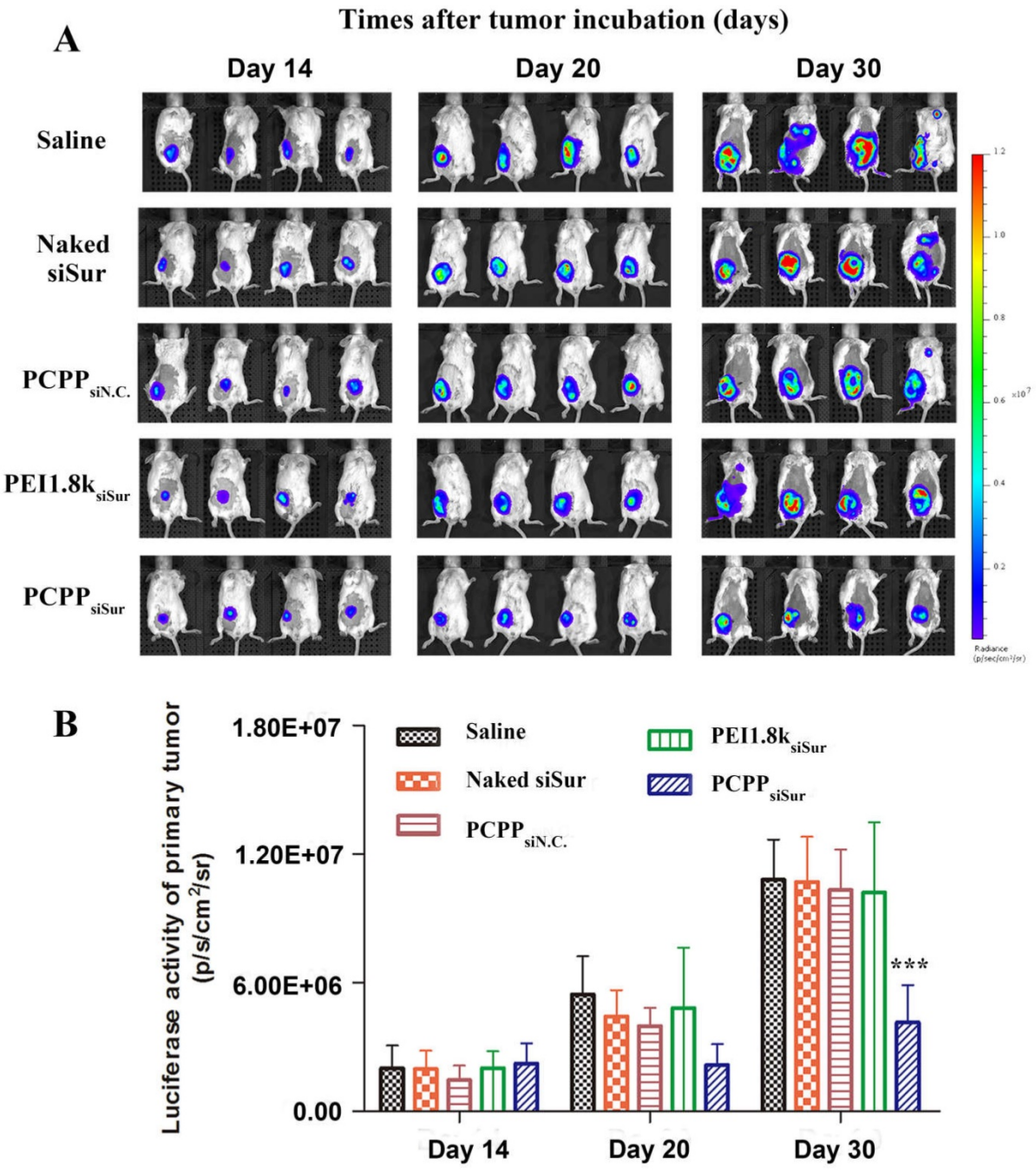

Figure 8. Effects of different siSur-loaded nanoparticles on metastasis burden in 4T1-Luc tumor-bearing mice. (A) Typical bioluminescent images of mice during the treatment with saline, naked siSur, $PCPP_{siN.C}$, $PEI1.8k_{siSur}$ or $PCPP_{siSur}$. (B) Quantitative estimation of metastases progression by bioluminescent imaging analysis (n=4, *** P <0.001).

Since metastasis is the primary cause of dying from carcinoma and aberrant overexpression of SA is closely related to the tumorigenic and metastatic potential of cancers, we investigated the tumor metastasis of mice besides monitoring the tumor growth. Here, we chose the 4T1 spontaneous metastasis model. As we know, trustworthy animal models are vital for evaluating therapy effect and defining tumor metastasis paradigms. Compared to transplantable tumor models, orthotopic and spontaneous metastasis models are usually recommended, because they mimic the organ-specific physiology feature of cancer and incorporate micro-environmental interactions[39, 40]. 4T1 mammary carcinoma cell is a mouse syngeneic mammary adenocarcinoma. It is one of the few breast carcinoma cell lines that models the development of metastatic disease due to the presence of an intact immune system. When introduced orthotopically, 4T1 tumor can spontaneously metastasize from original sites to distant organs via the lymphatic invasion and hematogenous pathway [35]. Moreover, compared

with other animal models whose tumorigenesis do not parallel their human counterparts, 4T1 tumors share a lot of features with human mammary carcinomas. After inoculated orthotopically, 4T1 cells spontaneously metastasize to the same sites as human breast carcinoma. This facilitates 4T1 model suitable for investigating metastatic cancer in immunocompetent mice[35]. From our results of in vivo anti-metastatic experiments, $PCPP_{siSur}$ nanoparticles exhibited higher efficacy on suppressing tumor growth and metastasis compared to the control groups, which is correlated with enhanced accumulation in tumors.

Conclusion

In order to achieve efficient siRNA-mediated gene silencing, we have engineered a PBA-based pH-responsive nanovector for targeted delivery and controlled release of siRNA. In our design, the PCPP/siRNA nanoparticle was constructed with three features: (1) a detachable PEG-shell to "shield" the PBA ligand in systemic circulation with the aim of reducing its "off-target effect"; (2) enhanced cellular internalization through "exposed" intact PBA moiety binding with overexpressed sialic acid moiety on cancer cells; (3) a compact cross-linked core due to the dual roles of siRNAs. Herein, PBA plays a key role that had dual functions: forming pH-liable linkers with *cis*-diols and targeting the SA-terminated sugar chains on cancer cells. Our results illustrated that PCPP nanovector could condense siRNA to form stable nanoparticles and facilitate siRNA into target cells to exert RNA interference effects. Most importantly, treatments with survivin gene-specific $PCPP_{siSur}$ nanoparticles have sharply increased apoptotic cells and enhanced inhibitory effect on cell

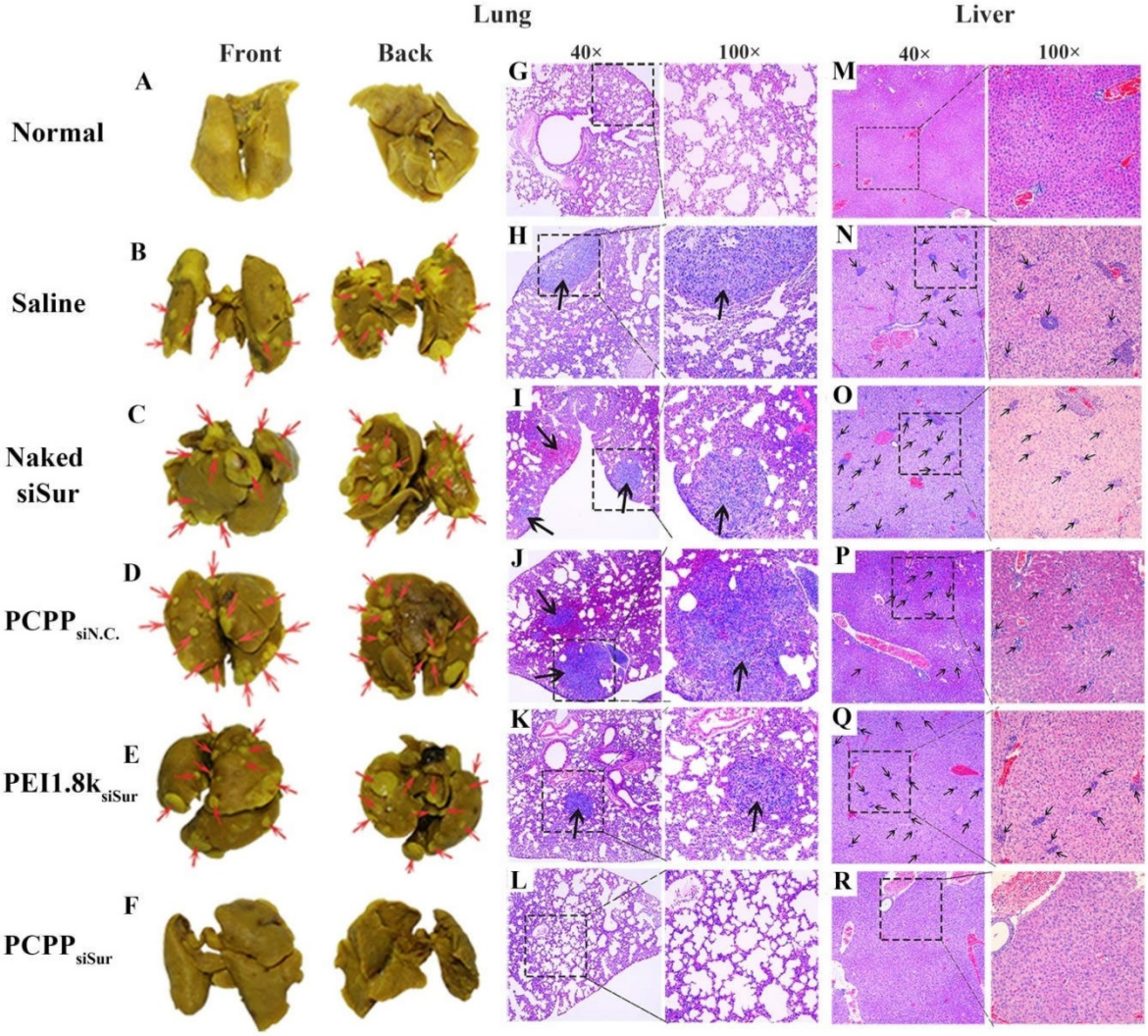

Figure 9. Representative optical photos of lung separated from 4T1-Luc tumor-bearing mice treated with different formulations (B-F) and the red arrows point out lung metastasis nodules. Typical histopathologic examination of lungs (H-L) and livers (N-R) of 4T1-Luc tumor-bearing mice receiving saline, naked siSur, $PCPP_{siN.C}$, $PEI1.8k_{siSur}$ or $PCPP_{siSur}$ respectively at different magnifications. The black arrows point out the metastatic foci in lung and liver tissues. The specimens from normal mouse were taken as controls (A, G, M).

migration/invasion in vitro. Benefiting from the detachable PEG modification and the sialic acid receptor-mediated cellular uptake, $PCPP_{siSur}$ nanoparticles improved the accumulation of siRNA in tumor sites after intravenous administration, which led to the effective inhibition on 4T1 orthotopic tumor growth and its distant metastasis. Thus, PCPP could serve as be a promising siRNA nanovector for treating metastatic breast cancer.

Abbreviations

PBA: phenylboronic acid; SA: sialic acid; PEG-Cat: catechol group modified poly(ethylene glycol); PEI-PBA: PBA-terminated polyethylenimine; PCPP: mPEG-CPB-PEI; siRNA: small interfering RNA; siN.C.: siRNAs of nonsense sequences; siLuc: siRNA of anti-luciferase gene; siSur: siRNA of anti-survivin gene; CLSM: confocal laser scanning microscopy; SNA: sambubus nigra lectin; WGA: wheat germ agglutinin; MAA: maackla amurensis lectin; Neu5Ac: N-acetylneuraminic acid.

Supplementary Material

Supplementary material, scheme and figures.
http://www.thno.org/v07p0357s1.pdf

Acknowledgments

This work was financially supported by Beijing Natural Science Foundation (No. 2141004 and 7142114), National Natural Science Foundation of China (No. 81373342) and Beijing Key Laboratory of Drug Delivery Technology and Novel Formulations, Institute of Materia Medica, Chinese Academy of Medical Sciences and Peking Union Medical College.

Competing Interests

The authors have declared that no competing interest exists.

References

1. Parker B, Sukumar S. Distant metastasis in breast cancer: molecular mechanisms and therapeutic targets. Cancer Biol Ther. 2003; 2: 14-21.
2. Hauselmann I, Borsig L. Altered tumor-cell glycosylation promotes metastasis. Front Oncol. 2014; 4: 28.
3. Varki A. Sialic acids in human health and disease. Trends Mol Med. 2008; 14: 351-60.
4. Matsumoto A, Cabral H, Sato N, Kataoka K, Miyahara Y. Assessment of tumor metastasis by the direct determination of cell-membrane sialic acid expression. Angew Chem Int Ed Engl. 2010; 49: 5494-7.
5. Bull C, Boltje TJ, van Dinther EA, Peters T, de Graaf AM, Leusen JH, et al. Targeted delivery of a sialic acid-blocking glycomimetic to cancer cells inhibits metastatic spread. ACS Nano. 2015; 9: 733-45.
6. Deshayes S, Cabral H, Ishii T, Miura Y, Kobayashi S, Yamashita T, et al. Phenylboronic acid-installed polymeric micelles for targeting sialylated epitopes in solid tumors. J Am Chem Soc. 2013; 135: 15501-7.
7. Ellis GA, Palte MJ, Raines RT. Boronate-mediated biologic delivery. J Am Chem Soc. 2012; 134: 3631-4.
8. Ji M, Li P, Sheng N, Liu L, Pan H, Wang C, et al. Sialic Acid-Targeted Nanovectors with Phenylboronic Acid-Grafted Polyethylenimine Robustly Enhance siRNA-Based Cancer Therapy. ACS applied materials & interfaces. 2016; 8: 9565-76.
9. Wang X, Tang H, Wang C, Zhang J, Wu W, Jiang X. Phenylboronic Acid-Mediated Tumor Targeting of Chitosan Nanoparticles. Theranostics. 2016; 6: 1378-92.
10. Singh N, Willson RC. Boronate affinity adsorption of RNA: possible role of conformational changes. J Chromatogr A. 1999; 840: 205-13.
11. Naito M, Ishii T, Matsumoto A, Miyata K, Miyahara Y, Kataoka K. A phenylboronate-functionalized polyion complex micelle for ATP-triggered release of siRNA. Angew Chem Int Ed Engl. 2012; 51: 10751-5.
12. Shankar P, Manjunath N, Lieberman J. The prospect of silencing disease using RNA interference. JAMA. 2005; 293: 1367-73.
13. Akhtar S, Benter IF. Nonviral delivery of synthetic siRNAs in vivo. J Clin Invest. 2007; 117: 3623-32.
14. Li Y, Xiao W, Xiao K, Berti L, Luo J, Tseng HP, et al. Well-defined, reversible boronate crosslinked nanocarriers for targeted drug delivery in response to acidic pH values and cis-diols. Angew Chem Int Ed Engl. 2012; 51: 2864-9.
15. Paszek MJ, DuFort CC, Rossier O, Bainer R, Mouw JK, Godula K, et al. The cancer glycocalyx mechanically primes integrin-mediated growth and survival. Nature. 2014; 511: 319-25.
16. Zhu JY, Zeng X, Qin SY, Wan SS, Jia HZ, Zhuo RX, et al. Acidity-responsive gene delivery for "superfast" nuclear translocation and transfection with high efficiency. Biomaterials. 2016; 83: 79-92.
17. Yang B, Jia H, Wang X, Chen S, Zhang X, Zhuo R, et al. Self-assembled vehicle construction via boronic acid coupling and host-guest interaction for serum-tolerant DNA transport and pH-responsive drug delivery. Advanced healthcare materials. 2014; 3: 596-608.
18. Yang F, Huang W, Li Y, Liu S, Jin M, Wang Y, et al. Anti-tumor effects in mice induced by survivin-targeted siRNA delivered through polysaccharide nanoparticles. Biomaterials. 2013; 34: 5689-99.
19. Ma X, Cheng Z, Jin Y, Liang X, Yang X, Dai Z, et al. SM5-1-conjugated PLA nanoparticles loaded with 5-fluorouracil for targeted hepatocellular carcinoma imaging and therapy. Biomaterials. 2014; 35: 2878-89.
20. Ren J, Zhang Y, Zhang J, Gao H, Liu G, Ma R, et al. pH/sugar dual responsive core-cross-linked PIC micelles for enhanced intracellular protein delivery. Biomacromolecules. 2013; 14: 3434-43.
21. Kim J, Lee YM, Kim H, Park D, Kim J, Kim WJ. Phenylboronic acid-sugar grafted polymer architecture as a dual stimuli-responsive gene carrier for targeted anti-angiogenic tumor therapy. Biomaterials. 2016; 75: 102-11.
22. Yan J, Springsteen G, Deeter S, Wang B. The relationship among pKa, pH, and binding constants in the interactions between boronic acids and diols—it is not as simple as it appears. Tetrahedron. 2004; 60: 11205-9.
23. Zhao C, Deng H, Xu J, Li S, Zhong L, Shao L, et al. "Sheddable" PEG-lipid to balance the contradiction of PEGylation between long circulation and poor uptake. Nanoscale. 2016; 8: 10832-42.
24. Ambardekar VV, Han HY, Varney ML, Vinogradov SV, Singh RK, Vetro JA. The modification of siRNA with 3' cholesterol to increase nuclease protection and suppression of native mRNA by select siRNA polyplexes. Biomaterials. 2011; 32: 1404-11.
25. Schultz MJ, Swindall AF, Bellis SL. Regulation of the metastatic cell phenotype by sialylated glycans. Cancer Metastasis Rev. 2012; 31: 501-18.
26. Fuster MM, Esko JD. The sweet and sour of cancer: glycans as novel therapeutic targets. Nat Rev Cancer. 2005; 5: 526-42.
27. Ambrosini G, Adida C, Altieri DC. A novel anti-apoptosis gene, survivin, expressed in cancer and lymphoma. Nat Med. 1997; 3: 917-21.
28. Yang Q, Zhang Z, Mei W, Sun F. A novel ruthenium(II)-polypyridyl complex inhibits cell proliferation and induces cell apoptosis by impairing DNA damage repair. J Chemother. 2014; 26: 235-42.
29. Ernsting MJ, Tang WL, MacCallum NW, Li SD. Preclinical pharmacokinetic, biodistribution, and anti-cancer efficacy studies of a docetaxel-carboxymethylcellulose nanoparticle in mouse models. Biomaterials. 2012; 33: 1445-54.
30. Bao Y, Jin Y, Chivukula P, Zhang J, Liu Y, Liu J, et al. Effect of PEGylation on biodistribution and gene silencing of siRNA/lipid nanoparticle complexes. Pharm Res. 2013; 30: 342-51.
31. Williams MC. Endocytosis in alveolar type II cells: effect of charge and size of tracers. Proc Natl Acad Sci U S A. 1984; 81: 6054-8.
32. Petros RA, DeSimone JM. Strategies in the design of nanoparticles for therapeutic applications. Nat Rev Drug Discov. 2010; 9: 615-27.
33. Davis ME, Chen ZG, Shin DM. Nanoparticle therapeutics: an emerging treatment modality for cancer. Nat Rev Drug Discov. 2008; 7: 771-82.
34. Furumoto K, Yokoe J, Ogawara K, Amano S, Takaguchi M, Higaki K, et al. Effect of coupling of albumin onto surface of PEG liposome on its in vivo disposition. Int J Pharm. 2007; 329: 110-6.
35. Tao K, Fang M, Alroy J, Sahagian GG. Imagable 4T1 model for the study of late stage breast cancer. BMC Cancer. 2008; 8: 228.
36. Jenkins DE, Yu SF, Hornig YS, Purchio T, Contag PR. In vivo monitoring of tumor relapse and metastasis using bioluminescent PC-3M-luc-C6 cells in murine models of human prostate cancer. Clin Exp Metastasis. 2003; 20: 745-56.
37. Lelekakis M, Moseley JM, Martin TJ, Hards D, Williams E, Ho P, et al. A novel orthotopic model of breast cancer metastasis to bone. Clin Exp Metastasis. 1999; 17: 163-70.
38. Aslakson CJ, Miller FR. Selective events in the metastatic process defined by analysis of the sequential dissemination of subpopulations of a mouse mammary tumor. Cancer Res. 1992; 52: 1399-405.

39. Talmadge JE, Singh RK, Fidler IJ, Raz A. Murine models to evaluate novel and conventional therapeutic strategies for cancer. Am J Pathol. 2007; 170: 793-804.
40. Ostrand-Rosenberg S. Animal models of tumor immunity, immunotherapy and cancer vaccines. Curr Opin Immunol. 2004; 16: 143-50.